Journal of
Hydroinformatics

 Journal of Hydroinformatics Vol 25 No 2, 451 doi: 10.2166/hydro.2023.162

A method of estimating imperviousness for the catchment modelling of urban environments

Siming Gong *, James Ball and Nicholas Surawski

School of Civil and Environmental Engineering, University of Technology Sydney, Sydney, Australia
*Corresponding author. E-mail: siming.gong@student.uts.edu.au

SG, 0000-0003-4244-1181; JB, 0000-0001-8342-1916; NS, 0000-0003-2584-1044

ABSTRACT

Urban impervious surfaces, a symbol of urbanisation, have permanently changed urban hydrology behaviour and play a critical role in modelling rainfall-runoff process. The distribution pattern of impervious surfaces is intrinsically connected with functional land zoning schemes. However, estimating impervious fractions for catchment modelling is becoming increasingly difficult due to intricate land zoning categories and heterogeneous land use land cover (LULC) during urbanisation. This study demonstrates an integrated approach of deep learning (DL) and grid sampling method to overcome the challenges of LULC classification, sample standardisation and statistical sample extraction. The classified impervious features were extracted within the land zoning scope and translated into polynomial functions using a probability-fitting approach to measure the occurrence likelihood distribution of samples' impervious fraction. Then, we use the information entropy (IE) to evaluate prediction stability by quantifying the condition entropy and information gain (IG) from each functional land zones to the occurrence likelihood of different impervious fraction intervals. The DL model shows robust LULC prediction, while probability-fitting study of impervious samples reflects the distribution differential of impervious fractions under the land zoning categories. The IE stability test shows a robust approach that clarifies different confident ranges of imperviousness estimation based on land zoning information.

Key words: catchment modelling, deep learning, information entropy, land use land cover (LULC), probability-fitting

HIGHLIGHTS

- Using DL techniques to classify and segment land use land cover (LULC) from the remote sensing imagery of a large urban catchment (total area: 4,348 ha) and determine impervious LULC classes.
- The urban functional land zoning concept was involved to define the impervious feature extraction and analysis scope.
- The IE concept was introduced to assess the stability of results and to quantify confidence ranges for different land zoning categories.

GRAPHICAL ABSTRACT

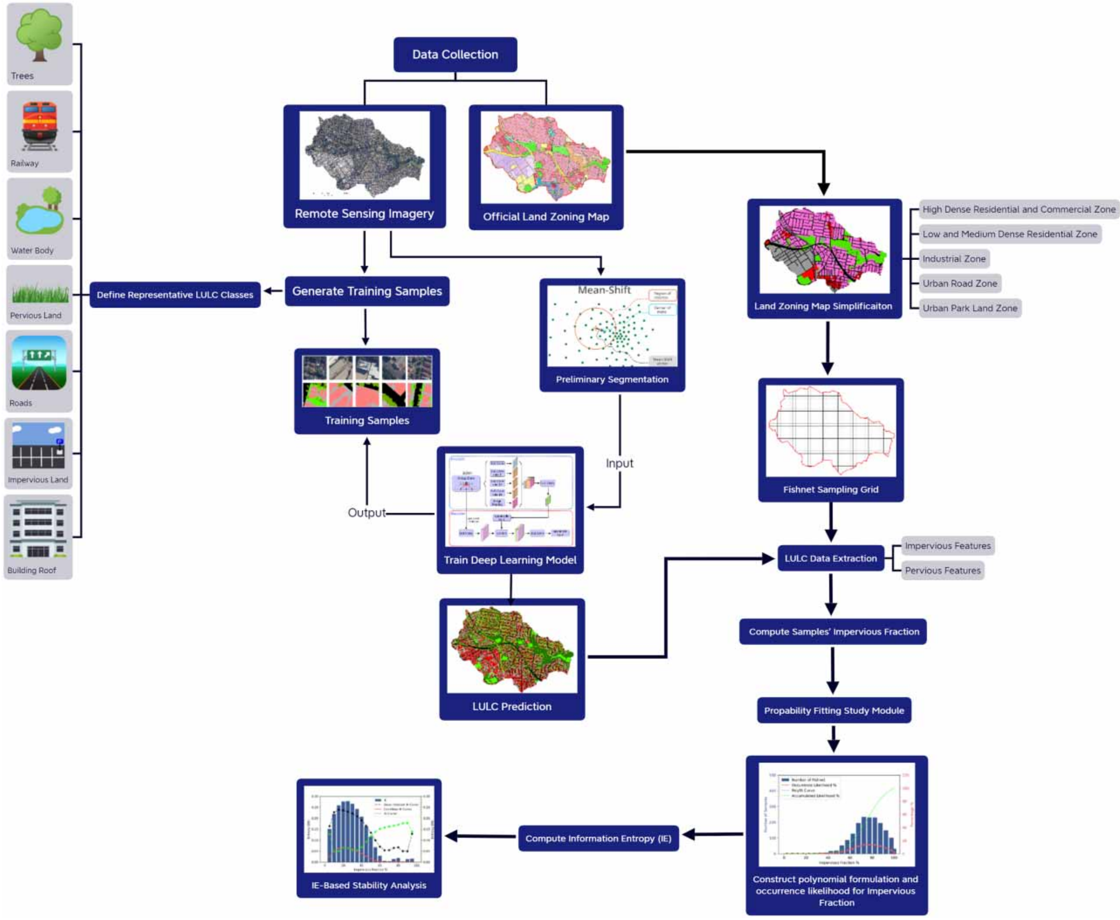

1. INTRODUCTION

The world is experiencing rapid urbanisation with the growth of the urban population and the expansion of urban areas (Andersen 2013). According to a prediction published in the Economist, by the middle of the 21st century, the proportion of people living in urban areas will reach 64 and 86% for developing and developed countries, respectively (Grimond 2007). To meet the urbanisation demand, natural vegetated lands are continually replaced by impervious surfaces such as asphalt roads, buildings and parking lots (Jensen & Cowen 1999), interrupting water infiltration and weakening the flood resilience of the natural catchment. In urban environments, impervious surfaces are dominant runoff producers under very frequent and frequent rainfall events due to the minor depression storage, interception and infiltration losses, where the runoff flow rate and volume are significantly higher than the same-size rural catchments (Ball *et al.* 2019). The impervious runoff examination for 763 rainfall events in 26 urban catchments showed that the average initial loss of 70% of study catchments was equal to or less than 1 mm (Boyd *et al.* 1993), which corroborated the dominant role of impervious surfaces in the runoff generation of urban catchments. However, the expansion of urban impervious surfaces will inevitably lead to water issues in those urban environments. Urban flooding caused by frequent rainfall is a common phenomenon worldwide and is getting severe due to objective factors like unscientific development, rapid urbanisation and climate change (Jamali *et al.* 2018; Huang *et al.* 2021). Therefore, urban impervious surfaces and their impact on flood resilience have become a unified theme that a scientifically planned impervious fraction must be considered during urbanisation (Weng 2012).

Limited by the current hydrologic data monitoring and measurement techniques, catchment modelling is one of the most popular approaches to simulating catchment rainfall–runoff process (Beven 2012), where most catchment modelling systems adopt impervious fractions as the input parameter to quantify runoff generation. Spatial variability, like changes in land use land cover (LULC), is strongly correlated with the hydrological and hydraulic response of the catchment. Therefore, the spatial variability of LULC is an innegligible issue when modelling an urban catchment. However, the existing catchment imperviousness estimation approaches provide a challenge for the development of reproducible and efficient workflows in the provision of estimates of impervious fraction values.

Estimation of the catchment response will be based on the available data. However, for potential future development within a catchment, details of the LULC are not available until the development has been undertaken. This is where the problem for catchment managers is generated: this is further complicated by an inability to reverse development once it has occurred. Therefore, there is a need for a catchment manager to estimate future catchment responses for development conditions that have not yet occurred. This is possible with the novel and innovative approach proposed herein.

Urban planning is a crucial phase of urbanisation that sets the tone and provides scientific advice for the city's future development, where land zoning is one of the most commonly used urban planning schemas to determine development patterns, environmental protection strategies and social and economic activities. In urban environments, the catchment impervious fraction is closely tied to the functional land zone to which it belongs. For example, the latest version of the Australia New South Wales (NSW) local environmental plan (LEP) making guideline proposes seven urban land use categories to standardise urban planning and development. These categories are residential zones, commercial zones, industrial zones, special purpose zones, recreation zones and environment protection zones (NSW Government 2021). Similarly, the American Planning Association (ASA) employed the optimum land use patterns theory to classify urban land uses as social, economic, functional and environmental (Duranton & Puga 2015). The Organisation for Economic Cooperation and Development (OECD) of the United Kingdom outlined a long-term vision of land development for the next 30 years in the national planning framework (NPF) and the regional development strategy, which support all levels of government to make spatial-related strategies under the framework and provide essential information (e.g. impervious rate) for all stakeholders interested in local development (OECD 2017).

The acquisition methods of impervious data for catchment modelling purposes can be summarised into two categories: manual and automatic. The manual method refers to delineating and extracting geometric elements of impervious features using geographic information system (GIS) tools through human cognition of impervious areas from remote sensing imagery (Slonecker *et al.* 2001). The manual method is more accurate than the automatic method, when combined with a field survey. Nevertheless, this accuracy sorely relies on the subjectivity and experience of the modeller and is usually accompanied by a massive data acquisition and interpretation workload, which limits the scope of its application, such as in large urban catchments (Mohapatra & Wu 2010; Weng 2012).

In recent years, the automatic impervious data acquisition method has sparked heated discussion in both academia and industry, as a result of the growing demand for large-area catchment models and an increasing heterogeneity of land use land cover (LULC) in urban catchments. The availability of remote sensing data is the core of the automatic acquisition method that extracts the spatial geometry of impervious features by analysing the spectral and texture features of LULC in remote sensing images. Remote sensors with sensitive spectral resolution can automatically distinguish the reflected spectral wavelengths of LULCs from the entire radiation spectrum and render the different LULCs to extract impervious features in post-image processing (Slonecker *et al.* 2001). For example, while the spectrum-based impervious features extraction approaches for pixel and object of remote sensing imagery have been proposed and achieved excellent performance in various application fields (Flanagan & Civco 2001; Yang *et al.* 2003; Yuan *et al.* 2008; Van de Voorde *et al.* 2009), but still require to invest many human resources in data interpretation at the feature extraction stage (Wu & Murray 2003). In the recent decade, urban impervious feature classification and extraction have entered a new era with the development of remote sensing databases and machine learning (ML) algorithms. The convolutional neural network (CNN)-based ML models resolved the drawbacks (e.g. salt-pepper noise) of spectrum-based classification approaches and achieved high precision and automaticity in classifying and segmenting remote sensing images, especially when dealing with some areas with high heterogeneous LULC. For example, Li *et al.* (2019) used an ML-based approach to distinguish the types of urban built-up areas with an overall accuracy of 95%. Xu *et al.* (2018) utilised the Res-Unet model to extract buildings' footprints from the high-resolution remote sensing imagery of Vaihingen and Potsdam. Zhang *et al.* (2018) developed an integrated approach of the multilayer perceptron (MLP) and CNN to classify LULC of urban remote sensing imagery and obtained an outstanding precision (classification accuracy of 90.93%) and robust performance (Kappa coefficient of 3.68) compared with the other tested approaches.

Catchment modelling parameter sets can be classified as measured or inferred, with the catchment impervious fraction belonging to the measured parameter set and playing a crucial role in deducing dimensionless inferred parameters such as depression storage and Manning's value (Choi & Ball 2002). The extracted impervious data can be interpreted and transported to the catchment model as input parameters to simulate the catchment rainfall–runoff process, identify the flood risks under existing catchment conditions and further guide urban development. However, there is a specific information hysteresis in guiding urban development or flood mitigation by modelling the existing catchment scenarios as urban is a dynamic system with the changing of LULC every day (Chen *et al.* 2009). A prospective catchment model can predict catchment hydrology in the post-development scenarios and enhance the hydrologic evaluation capacity of city planners in defining functional zones for pre-developed catchments if we can build the prospective model with scientifically estimated imperviousness before it is urbanised. In addition, determining the impervious fraction of different functional land zoning categories is a grand challenge to catchment modellers, especially when dealing with large urban catchments and heterogeneous LULC (Salvadore *et al.* 2015). A reliable zone-based impervious fraction estimation approach can not only initialise catchment models but also support building harmony between land use, water and environments, such as legislative constraints on land use, building size and population density based on the natural characteristics of a land lot (National Research Council 2009; Byrne *et al.* 2014). Therefore, the research on the impervious features of different land zones has considerable significance for enhancing catchment modelling capacity, guiding urban planning and assessing the flood risks of catchment urbanisation.

This paper proposes a prior probability approach to analyse the impervious fraction of five representative functional urban land zones in Australia, including low- to medium-density residential, high-density and commercial residential, industrial, urban green land and urban road. Five urban catchments within the Greater Sydney area are selected as the database to extract impervious surfaces for evaluating the distribution of the impervious fraction of the five functional land zones. The section 'Methodology' first describes the study catchment conditions and adopted datasets in this study, followed by the workflow of LULC classification, impervious features extraction, samples' probability-fitting and the outputs stability study. The 'Results and discussion' section demonstrates the predicted LULC maps, occurrence likelihood distribution of impervious fraction and information entropy (IE) distribution under different land zoning categories. The key findings and research prospects are involved in the 'Conclusion'.

2. METHODOLOGY

2.1. Outline of methodology

The proposed methodology consists of four components: image classification, impervious feature extraction, probability-fitting study and data stability analysis. Firstly, the approach proposed by Gong *et al.* (2022) was duplicated to conduct the imagery classification and segmentation. This study inherited the MeanShift algorithm to preliminary segment image objects by clustering pixel spectral information. In the deep learning (DL) module, the DeepLabV3+ (Chen *et al.* 2017) substituted Unet (Zhou *et al.* 2018) to classify the LULC information from the high-resolution imagery due to its better stability and consistency in predicting big datasets, as verified by Gong *et al.* (2022) and Yurtkulu *et al.* (2019). Then, the GIS spatial fusion approach was utilised to integrate the simplified land zoning and classified LULC maps (Tripp Corbin 2015). Secondly, a fishnet sampling GIS grid layer was created to adapt the format of the fundamental dataset, extract LULC features from the study catchment imagery and then export the statistical database for impervious and pervious samples. Finally, the computed distribution curves of the impervious feature were translated to IE for output stability analysis.

2.2. Study catchments

Five urban catchments in the Greater Sydney region of Australia were selected as sample catchments; each of the selected catchments contained different combinations of land zones with the urban planning legislation foundation of NSW, Australia. Figure 1 shows the location of these five urban catchments. Details of catchment names and areas are provided in Table 1. A common characteristic of the five urbanised catchments is heterogeneous LULC, which reflects similar LULC but different distribution patterns. As mixed land zoning catchments, all of the study catchments consist of various types of ground truth features, including houses, terraces, apartments, shopping centres, factories, sports fields and urban landscapes. The concentrated distribution of functional structures can be detected from the high-resolution remote sensing imagery of the five catchments, which means they have experienced or are experiencing land zoning and re-zoning development. In addition, the heterogeneous LULC of the study catchments will lead to difficulty in identifying and interpreting LULC information from the remote sensing

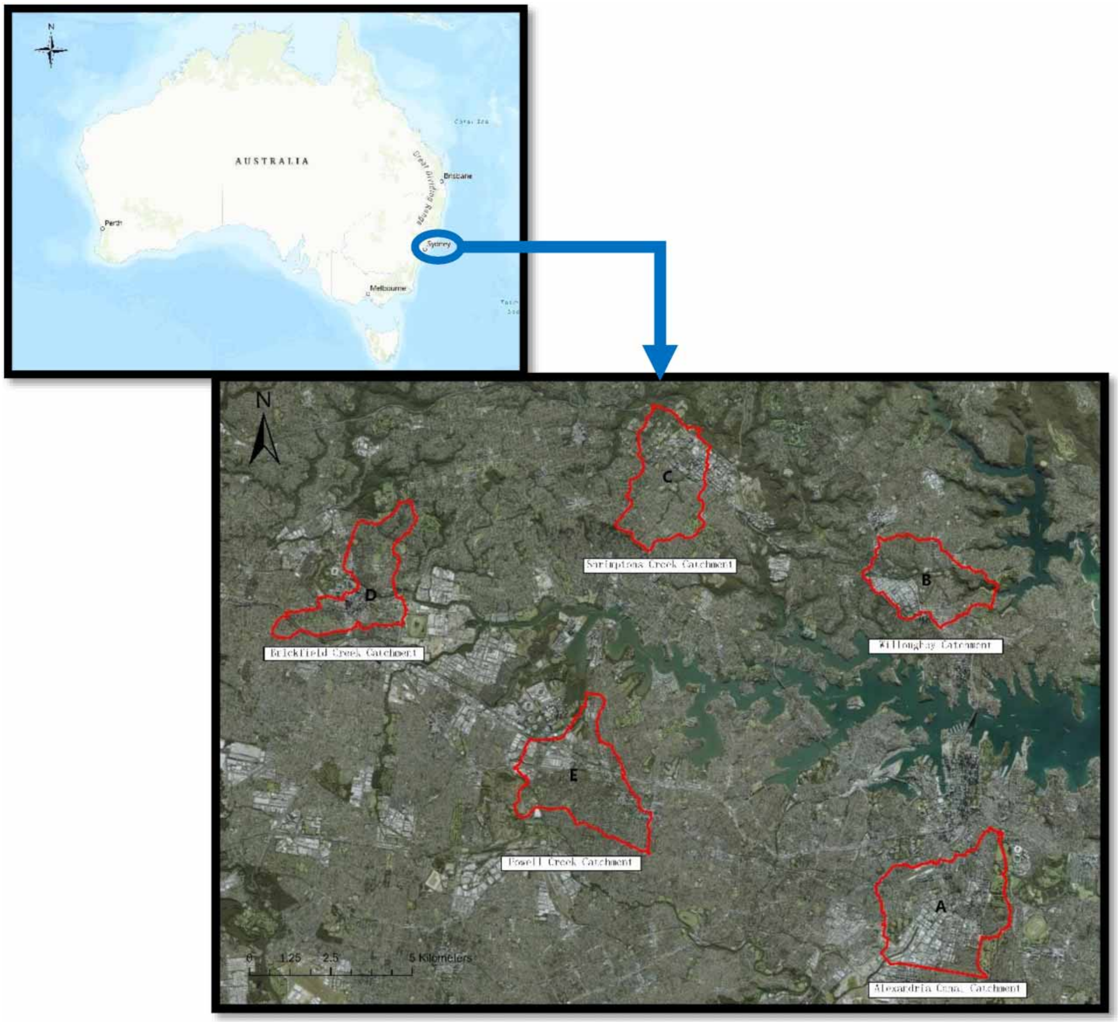

Figure 1 | Location of study catchments. (a) Alexandria Canal catchment; (b) Willoughby Creek catchment; (c) Shrmptons Creek catchment; (d) Brickfield Creek catchment and (e) Powell Creek catchment.

imagery, while using a land zoning map to group land use by functional attribute can significantly enlarge the sample amount and hence increase the robustness of the statistical model (Jiang 2010).

2.3. Data collection and preparation

The datasets used for this study include remote sensing imagery and land zoning maps. The spatial resolution of remote sensing imagery has experienced a significant evolution, from 80 m (Landsat-7), 30 m (Landsat-TM) and 10 m (SPOT) to 1.0 m

Table 1 | Study catchment areas

Catchment	Area (ha)
Alexandria Canal catchment	1,150
Powell Creek catchment	982
Willoughby Creek catchment	697
Shrmptons Creek catchment	802
Brickfield Creek catchment	717

(IKONOS) and 0.3 m (QuickBird) with global, multi-temporal and high-geometric resolution image sequences after decades of rapid development, which become the essential geospatial dataset for urban planning, resource development, ecological protection, catchment modelling and disaster prevention and mitigation (Chevrel *et al.* 1981; Johnston & Barson 1993; Toutin & Cheng 2002; Dial *et al.* 2003; Williams *et al.* 2006; Ball *et al.* 2019). The term spatial resolution implies the most acceptable object size that the remote sensor will detect on the ground, which does not translate into object recognition capacity but represents the information coverage area of one single pixel on the ground (Atkinson & Curran 1997). As the fundamental data, the high-resolution imagery is indispensable for generating the DL training set, classifying ground LULC and extracting impervious features. Selecting the appropriate spatial resolution and associated imagery product is the critical step in data preparation, where the pixel size must cover the majority of LULC features without overloading the training process.

The adopted remote sensing dataset of the study is the standard RGB (three bands: Red, Green and Blue) imagery fused by multiple metadata, including AAM, Jacobs Group Ausimage and Landsat, which was rendered and released by the Spatial Service Department of the NSW State Government (NSW Spatial Service 2021). The selected spatial resolution is 0.29 m per pixel width, referring to the minimum size of study catchments' LULC objects. According to Li *et al.* (2019), Weih & Riggan (2010) and Xu *et al.* (2018), less than 0.5 m pixel width has sufficient capacity to delineate textural features of LULC (e.g. single dwelling, plants) without losing their spectral information.

Functional land zoning is one of the most welcome urban planning approaches used in countries with abundant experience in city management, which plays a critical role in regulating the built markets and creating functional urban living spaces (Caves 2004; Mason 2012). Many municipalities and similar levels of government divide the urban areas into different sections and permit the construction of particular structures on the associated land zones to achieve the planned functional zoning purpose or a planned environmental friendly development. In practice, land zoning maps are usually drafted by local governments in response to delineating particular zones for various land use purposes, which play an essential role in promoting scientific, regulated and sustainable urban development (Gurran *et al.* 2015). In this study, land zoning maps occurred from the official database of local governments, including the City of Sydney (City of Sydney Council 2012), Willoughby (City of Willoughby Council 2012), Ryde (City of Ryde Council 2014), City of Parramatta (City of Parramatta Council 2011) and Strathfield (City of Strathfield Council 2012). Local deviations were found between the land zoning maps and actual land covers during the on-catchments investigation, which are caused by the lagging development and changing land zones. For example, the remote sensing image shows the factory building complex zoned as a residential area on its land zoning map since the development of the relevant residence has not yet been completed. Also, some attributes of land zoning maps with similar impervious fractions are uniformly considered in this study. For example, development in City of Sydney land zoning map, zone R5 (larger lots residential) and zone B3 (commercial core) are usually presented as residential–commercial mix buildings and have no significant differences in impervious fractions.

In summary, appropriate adjustment and correction for the official land zoning maps by referring to the actual ground cover of remote sensing imagery are essential to ensure the consistency and stability of the subsequent samples. This study merges the original land zoning subdivisions into five representative land zoning categories: high-density residential and commercial, low- to medium-density residential, industrial, urban roads and urban landscaping. This simplified land zoning pattern groups land subdivisions with similar impervious features without sacrificing their functional discrimination from the perspective of urban planning. The simplified land zoning maps are shown in Figure 5.

2.4. Imagery classification and segmentation

A DL-based imagery classification framework proposed by Gong *et al.* (2022) was reproduced to classify the LULC from the remote sensing imagery of the five study catchments. Seven typical urban LULC types were determined by site investigation and imagery observation to represent their ground features, which are trees, railways, waterbodies, pervious land, roads, impervious land and roofs, followed by labelling the associated LULC from the imagery to set up the ground truth side of DL training samples. The selected five urban catchments with heterogeneous LULC imply plenty of spectral and textural information in their remote sensing imagery, leading to time-consuming DL model processing. The clustering algorithm MeanShift (Comaniciu & Meer 2002) was utilised to group the pixels with similar spectral information for reducing the spectral and textural complexity and realise the initial segmentation of objects from the imagery. Then, the preliminary segmented images were conveyed to the input side of the deep neural network (DNN) classifier DeepLabV3+ (Chen *et al.* 2018) for training with the label ground truth features. After that, the trained DNN model was applied to predict LULC for the five study catchments. A workflow of MeanShift and DeepLabV3+ is shown in Figure 2.

2.5. Impervious features extraction

The dominant surface that generates runoff in an urban catchment is the impervious area under all kinds of rainfall events (from frequent to rare). In this study, the DeepLabV3+ DNN has classified the ground features of remote sensing imagery into the seven defined LULC classes, where railways, impervious ground, roads and roofs are grouped as impervious features due to their rapid rainfall response in urban environments. In contrast, trees and pervious land are treated as pervious features.

A fishnet sampling approach is proposed to extract impervious features from the predicated LULC maps of study catchments. Firstly, we created a mesh layer with a grid size of $100 \times 100\,\mathrm{m}^2$ to rasterise the entire area of the study catchments. The fishnet grid size is determined to be consistent with the average size of the large structures (e.g. factories and warehouses) in the study catchments so that one grid could cover homogeneous ground objects to the greatest extent without losing the samples' textural information and zonal diversity.

The classified LULC raster and simplified land zoning map were spatially joined to fuse land zoning extent and impervious features, where the LULC pixels are finely aligned with the land zoning area by projecting them to the same coordinate system. Meanwhile, the GIS clip tool was utilised to cut out the corresponding LULC data from the fused dataset. After that, the cropped fusion layer was subdivided by overlying the fishnet grid layer to sample the impervious features of each land zone at the catchment scale, which was accompanied by the occurrence of dissolved sample geometry due to the asynchronous data intersection process. Finally, the extracted samples will be grouped by land zoning categories and conveyed to the probability-fitting module for further analysis. An example of the fishnet sampling workflow is shown in Figure 3.

The impervious fraction of each grid sample is governed by its total impervious area (TIA) and the total aggregated area (TAA) of each dissolved sample element. Differing from the computation of TIA, urban road zones adopt the leaf area index (LAI), a dimensionless parameter that defines the ratio of the canopy area and ground surface area (Chen & Black 1992) to downscale

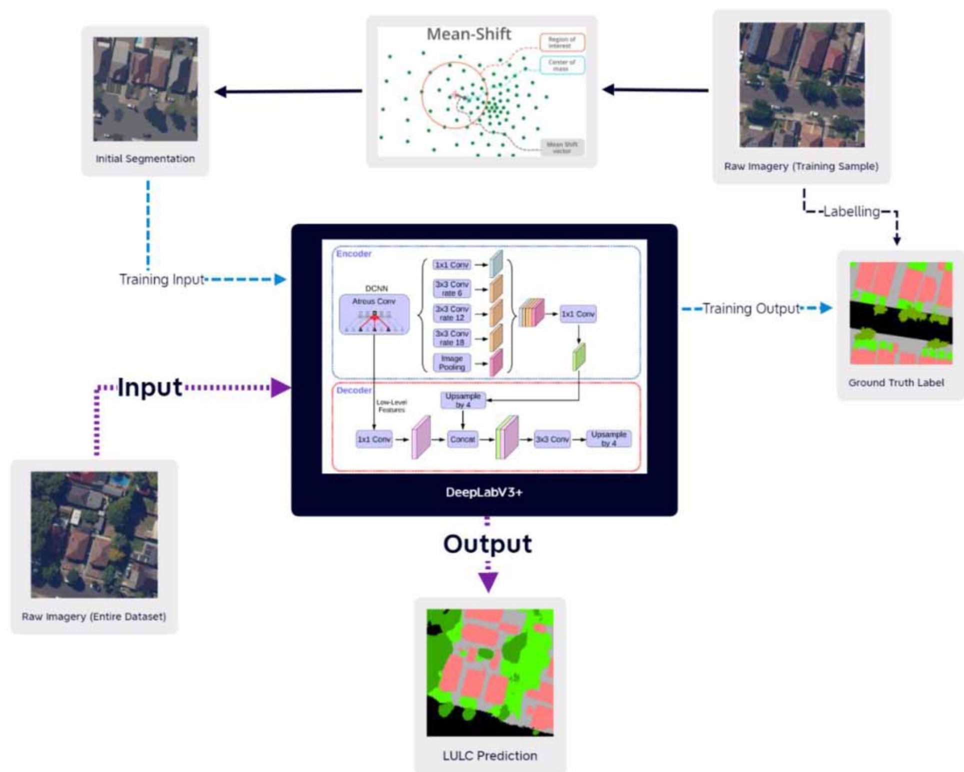

Figure 2 | Catchments imagery classification and segmentation workflow.

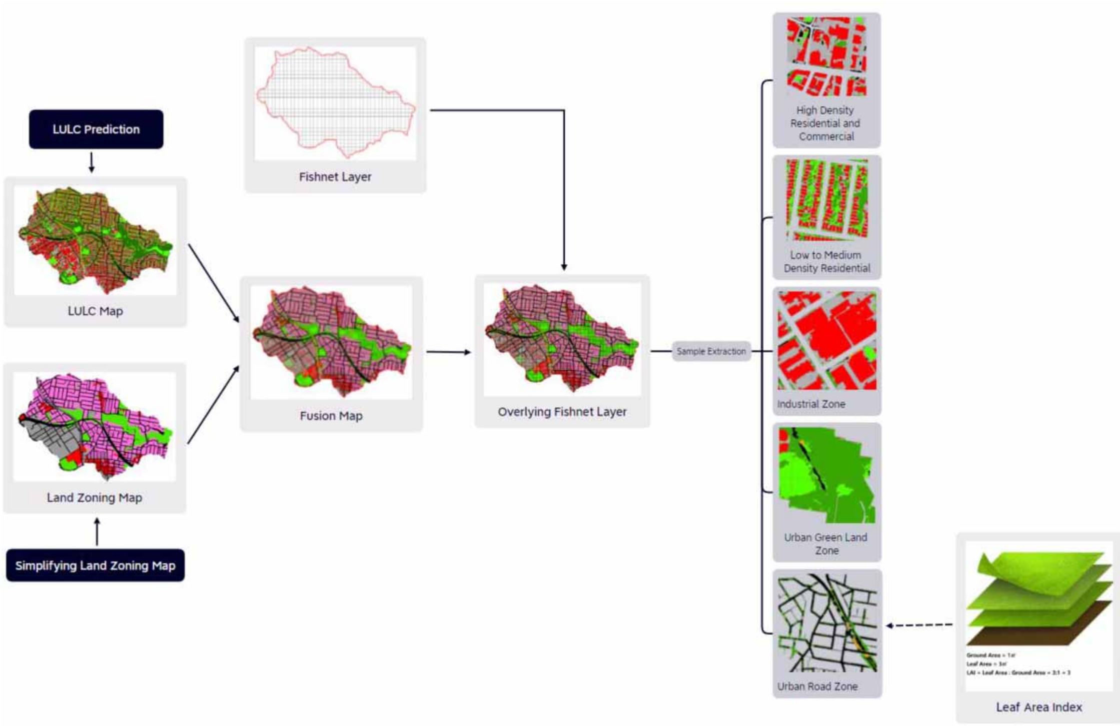

Figure 3 | Sketch of 'Fishnet' sampling approach.

the pervious area and further calculate the samples' impervious fraction, because applying the undecorated DNN segmentation results will greatly underestimate the impervious rate in road areas due to the obstruction of the border tree canopy observed from the remote sensing imagery. Therefore, LAI was involved in mitigating the error caused by tree canopy and estimating the pervious area of border trees. The LAI data of eucalyptus mixed hardwood (common tree species in Australia) was selected for this study and was obtained from the Geoscience Australia Portal managed by the Geoscience Australia department of the Australian Government (Geoscience Australia 2022). The governing equations of the sample's impervious fraction are expressed as:

$$TIA_i = \sum_{1}^{j} A_{imp} \tag{1}$$

$$TAA_{(i)} = \sum_{0}^{k} A_d \tag{2}$$

$$Impervious\ Fraction_i = \left(\frac{TIA_i}{TAA_i}\right) \times 100\% \tag{3}$$

$$GSA_{(tree)} = \frac{A_{tree}}{LAI} \tag{4}$$

$$Impervious\ Fraction_{i(urban\ road\ zone)} = \left[\frac{1 - (GSA_{tree} + A_{per})}{TAA_i}\right] \times 100\% \tag{5}$$

where A_{imp}, A_d and GSA_{tree} are the total impervious features area of the sample 'i', dissolved area of sample 'i' and ground surface area of sample 'i' belongs to urban road zone, respectively. 'j' is the classified LULC features and 'k' is the total number of dissolved pieces belonging to sample 'i'.

2.6. Sample probability-fitting study

The probability-fitting method is a numerical calculation method guided by probability and statistics theory that helps people deal with uncertainty in complex situations (Malz 1997). Establishing a probability model or stochastic process with a large number of random variables is the kernel of the probability-fitting method, assuming its parameters or numerical characteristics are equal to the solution of the problem by creating a joint distribution of possible outcomes resulting from the combination of the related variables (Tokuda *et al.* 2002). These parameters or numerical features will be translated to specified values or ranges as a final approximation of realistic scenarios (Metropolis & Ulam 1949). In catchment modelling, the determination of the model parameters is driven by probability to some extent instead of physical state since the continuous dynamic changing of the catchment, such as change of LULC, that is, the parameters take values from a range rather than a fixed number (Kuczera & Parent 1998).

In this study, the probability-fitting method was utilised as a quantitative probabilistic analysis tool to generate the likelihood and accumulated likelihood distribution of impervious fractions of each land zoning category.

- Firstly, determine the variables that represent the source of uncertainty. The land zoning attribute is defined as the study variable that groups study samples into five zoning categories: high-density residential and commercial zone, low- to medium residential zone, urban green land zone, industrial zone and urban road zone.
- Secondly, assume a distribution for each variable. In this case, the skewness distribution was assumed to conform to the samples' distribution as the constraint of the boundary condition.
- Thirdly, generate some iterations with possible realisations of each variable. As the study sample, the grid impervious fraction was transferred to the input side of the assumed distribution equations to realise iteration, where the whole impervious fraction domain (0–100%) was split into 20 fraction ranges with an increment of 5%.
- Finally, substitute all samples into the iteration to generate a joint likelihood distribution.

Considering a proportion of the area (no land zoning data) is erased during sample impervious feature extraction and resulting in the reduction of sample area compared with the preset sample area (1 ha), this study adopted the area reduction ratio of the sample area and the preset sample area as the quantity to count the number of samples.

2.7. Outputs stability analysis

Essentially, land zoning information has positive feedback for estimating the imperviousness of a plot; that is, the confidence range of the imperviousness of a plot can be further narrowed by knowing its land zoning information. The quantisation of land zoning information and its contribution to the impervious fraction distribution have significant meaning in exploring the validity of the probability-fitting model results.

In the 1940s, inspired by the theory of thermodynamics, Claude Elwood Shannon (1916–2001) invented the concept of IE by excluding redundancy from the average amount of information. IE resolves the question of information quantisation and clarifies the relationship between probability and information redundancy in the mathematic language (Núñez *et al.* 1996).

In catchment modelling, the imperviousness is determined by its natural attributes (e.g. urban or rural) without considering the contribution of any objective information such as climate and human activity. However, the heterogeneous LULC in the urban environment will lead to a great deal of uncertainty on imperviousness parameters and make associated values beyond the error tolerance of the general catchment modelling systems. This study borrows the concept of IE to quantify the information and correlated information gain (IG) of each land zoning category, where the gross impervious fraction likelihood is treated as the fundamental information quantity, and the land zoning-based impervious fraction likelihood is the additional information, namely IG. The workflow of output stability analysis is presented in Figure 4 and the IE formula is expressed as:

$$H(Y|X) = \sum_{x \in X} P(x) H(Y|X) = \sum_{x \in X} \sum_{y \in Y} P(x, y) \log \frac{1}{P(y|x)} \quad (6)$$

$$I(X; Y) = H(X) - H(YX) \quad (7)$$

where $P(x)$ and $H(Y|X)$ are conditional probabilities expressed as polynomial functions. X is catchment's natural attribute (urban) and Y is land zoning information. $I(X; Y)$ is the mutual information (MI) for quantifying the IG from the land zoning dataset.

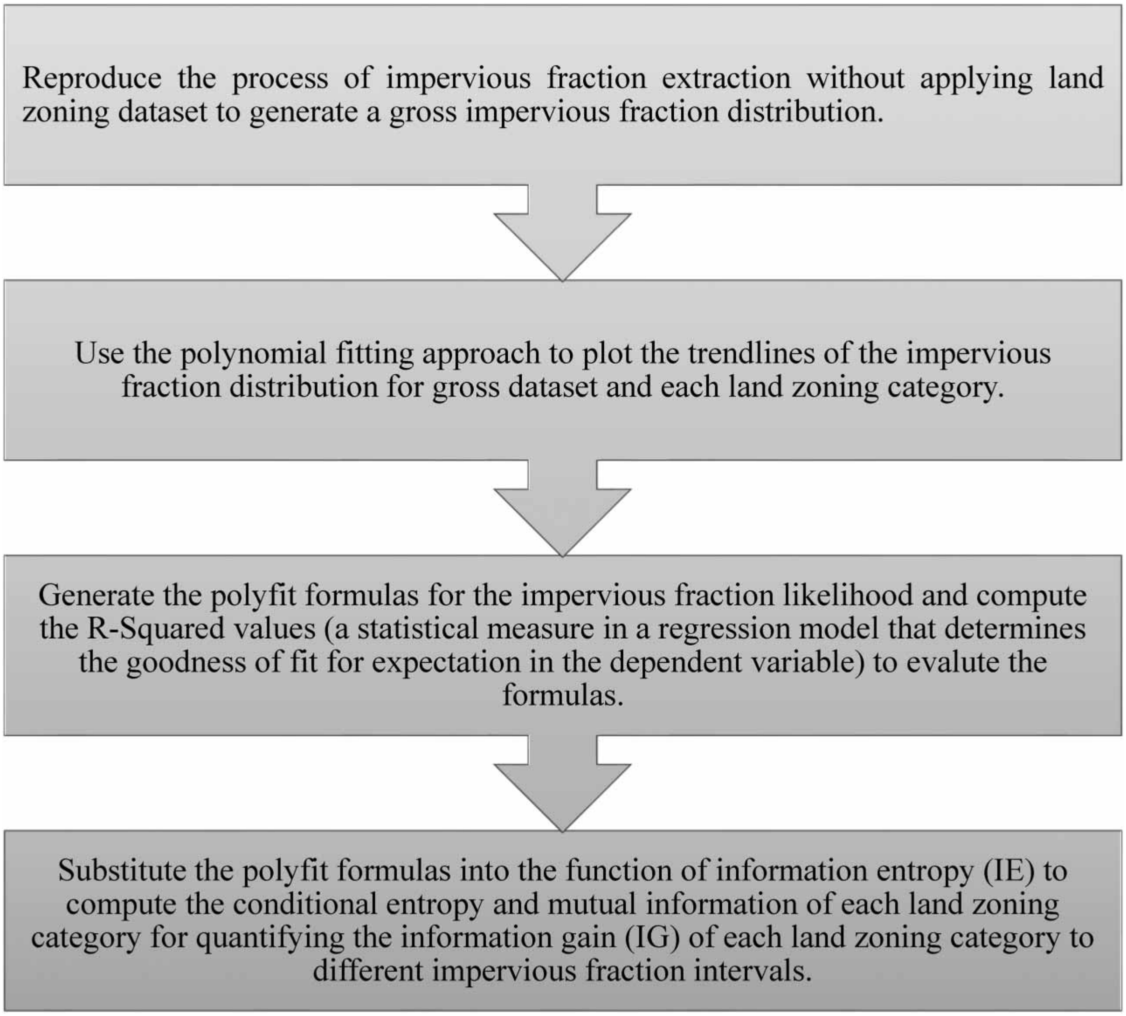

Figure 4 | Workflow of computing IE.

3. RESULTS AND DISCUSSION

3.1. Imagery outputs

The imagery processing outputs consist of two components: classified LULC maps and simplified land zoning maps. LULC maps describe the spatial distribution of ground features with detailed representative land cover classes in the study catchments. While the simplified land zoning maps eliminate the information unrelated to catchment imperviousness (e.g. administration and cadastre) from the original dataset by merging subdivisions that belong to the same land zoning attribute. As the inputs of the probability-fitting study, a high accuracy standard was considered to evaluate the LULC prediction performance of the DeepLabV3+. The two indicators, overall accuracy and Kappa coefficient, are applied to measure the prediction accuracy and reliability through the randomly distributed 500 checking points among the study catchments (Sim & Wright 2005). The Kappa coefficient (Stehman 1996), an index that can punish the 'bias' of the model, is adopted to assess prediction consistency. The prediction error within impervious LULC classes (roof, road, impervious land and railway) is ignored as they are unified during impervious feature extraction. Figure 5 shows the catchment's raw remote sensing imagery, simplified land zoning maps and the corresponding LULC prediction.

The accuracy assessment of LULC classification is presented in Table 2 by using the confusion matrix to compare the ground truth and DNN prediction. The overall prediction accuracy is 0.9073, where the impervious features, pervious land and trees achieved the prediction accuracy of 0.9634, 0.7422 and 0.8611, respectively. A robust LULC prediction

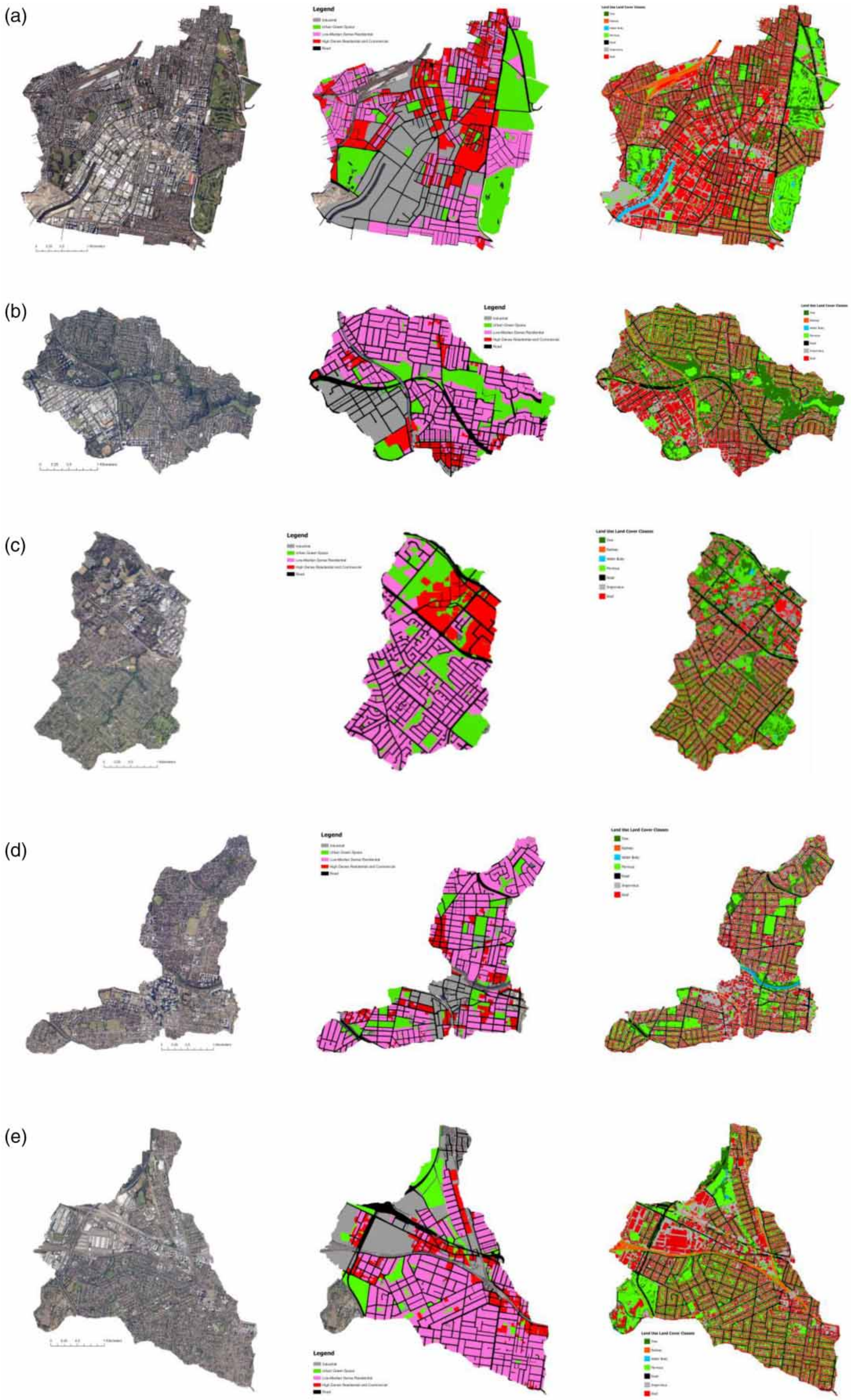

Figure 5 | Raw remote sensing imagery acquired in April 2019 was used to extract LULC data, while land zoning maps represented the planned land uses of the study catchments: (a) Alexandria Canal catchment; (b) Willoughby Creek catchment; (c) Shrmptons Creek catchment; (d) Brickfield Creek catchment; and (e) Powell Creek catchment.

Table 2 | Confusion matrix of DeepLabV3+ prediction accuracy assessment

Lulc class	Tree	Water body	Pervious	Impervious	Total	U_accuracy
Tree	62	0	10	6	78	0.8615
Water body	1	10	0	0	11	0.75
Pervious	6	0	72	6	84	0.8481
Impervious	3	0	15	316	334	0.9028
Total	72	10	97	328	507	
P_accuracy	0.8611	1	0.7422	0.9634		

Note: P_accuracy, prediction accuracy; U_accuracy, user accuracy; overall accuracy = 0.9073; Kappa = 0.8217.

model developed by Rwanga & Ndambuki (2017) was also assessed by using the confusion matrix and got a Kappa coefficient of 0.722. In this study, the Kappa coefficient (0.8217) qualifies as considerable, indicating that the proposed DL approach has consistent prediction performance among the defined LULC classes of the selected study catchments. The acceptable level of prediction accuracy varies depending on the available conditions, and most DL models consider 75% accuracy as the lowest boundary of excellent prediction (Li *et al.* 2019; He *et al.* 2020; Kiran 2020). In this study, the 0.9634 prediction accuracy of impervious features is sufficient to estimate parameters for simulating the rainfall–runoff process in urban catchments. Therefore, the outputs of impervious feature extraction are acceptably conveyed to the sampling process as the inputs of the probability-fitting study.

3.2. Probability-fitting outputs and polynomial curves

The LULC maps and simplified land zoning maps were transmitted to the fishnet sampling procedure to prepare the dataset for the probability-fitting study. The workflow is shown in Figure 3 and the governing equations for computing samples' impervious fractions are presented in Equations (3) and (5). The amount of fishnet samples is proportional to the area of different land zoning categories in the study catchment, which aligns with the theory of stratified random sampling for avoiding the 'bias' caused by the larger area land zoning category (e.g. low- to medium-density residential) (Vries 1986). Table 3 illustrates the number of raw and downscaled fishnet samples (after applying the area reduction ratio).

Figure 6 is plotted to describe the results of the probability-fitting study. Three elements, impervious fraction histogram, accumulated likelihood distribution and polynomial fitting curves, are involved in each figure to demonstrate the occurrence likelihood of each impervious fraction range with the effect of land zoning categories. Figure 6(a)–6(e) illustrates the diverse distribution scenarios of impervious fractions, which align with the realities of urban planning and construction. As mentioned in Section 2.6, the skewness distribution is assumed to fit the samples' impervious fraction distribution. This assumption is further verified to be correct by these figures. Therefore, it is appropriate to use a polynomial fitting method to generate the fitted curves of these distributions. Figure 6(f) is plotted to explore the general imperviousness condition of the five study catchments, where an urbanised picture is reflected by its impervious fraction distribution.

Table 3 | Number of raw and downscaled fishnet samples for each land zoning category and gross dataset

Land zoning	Raw sample amount	Downscaled sample amount
High-density residential and commercial	1,151	487
Low- to medium-residential	3,275	1,693
Industrial	1,073	567
Urban green land	1,645	647
Urban road	4,236	945
Gross data	5,166	4,647

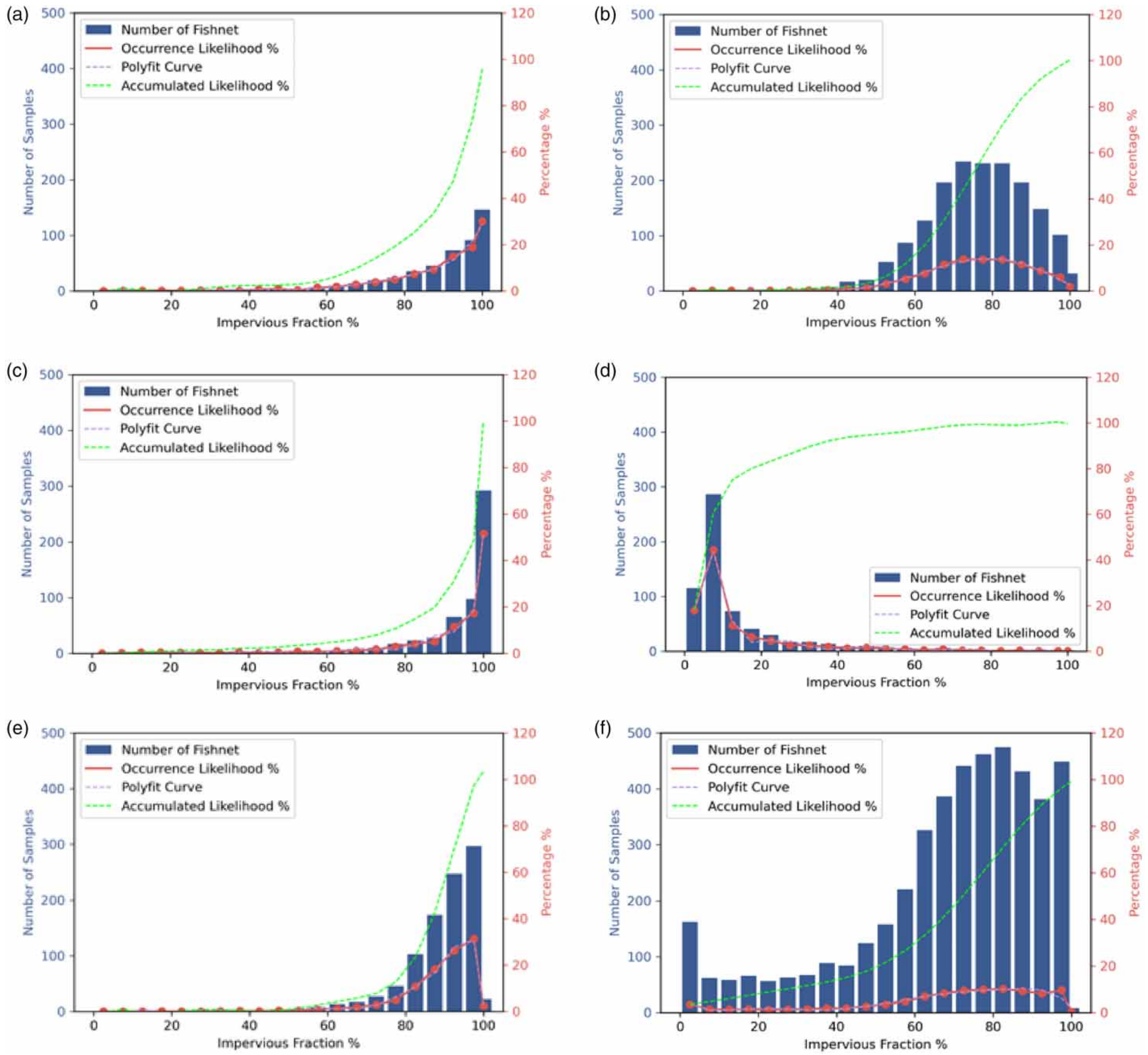

Figure 6 | Impervious fraction distribution: (a) High-density residential and commercial zone shows a strong imperviousness with a gradual increase from 70 to 100% and neglectable samples distributed between 0 and 60%; (b) Low to medium-density residential zone shows a concentrated distribution between 65 and 90%, with a peak of 80%; (c) Industrial zone demonstrates high imperviousness dominant characteristics, where most samples have an impervious fraction greater than 95%. (d) Urban green land zone illustrates a significant amount of pervious samples occupying the impervious fraction range from 0 to 20%; (e) Urban road zone presents moderate to high imperviousness (80–100%), which is affected by the pervious areas of green belt and border trees; and (f) Gross sample distribution exposes the high urbanised connotation of the five study catchments: most samples are scattered in the range of 60–100%, together with a bulge at 5% representing the urban landscape.

In catchment modelling, a distributed impervious fraction parameter set can be estimated using the functional polynomial fitting curves for any pre-developed urban catchment. For example, in urban planning, an area of the pre-developed catchment will not only be zoned for specified land use but also be divided into a number of land lots. These land zone-attributed lots can be mapped to the corresponding distribution curve as inputs to generate their impervious fraction numbers at the output side. These outputs are capable of better representing the imperviousness of the catchment after development with the increase of the input amount. This prior likelihood approach provides a new pattern to estimate the parameter of catchment impervious fraction for modelling catchment hydrology to guide the planning and development of urban catchments more effectively.

3.3. Information entropy evaluation

In this study, the polynomial fitting curves are used to generate the polynomial function of each land zoning category and translate them into probability functions for the IE formulas (6) and (7) in Section 2.7 to compute their values of conditional entropy and the IG. Table 4 lists the polynomial probability function of the gross dataset and five land zoning categories, where their R^2 values reflect the high goodness-of-fit of the polynomial function to the sample distribution. R^2 can take any value between 0 and 1, standing for the goodness-of-fit from low to high.

The results in Section 3.2 demonstrate the distinctive distribution patterns of impervious fraction likelihood under different land zoning categories, which has verified the selectivity enhancement spectrum of land zoning to the impervious fraction from the perspective of statistics. In this section, land zoning is informationised to quantify its contribution to different impervious fraction intervals using IE, conditional entropy and IG. The information amount of knowing one event's probability by measuring its IE, that the higher the probability, the lower the IE (Núñez *et al.* 1996; Volkenstein 2009). IE could be 0 when we know that an event will definitely happen (e.g. the sun rising from the east) because the amount of information required to judge the probability of this event is zero. When a new condition is involved in judging one event's occurrence, the enhancement degree of the event probability by the new condition is also different depending on its provided information amount, hence requiring the condition IE to measure it.

In this case, IE and condition IE represent the stability of impervious fraction estimation by knowing the LULC spatial distribution pattern and land zoning category, respectively. The IG is used to measure the information contribution of each land zoning category to the different impervious fraction intervals. Figure 7 shows the IE, condition IE and IG of the gross dataset and land zoning categories. The gross dataset, Figure 7(a), illustrates a more confident and stable imperviousness estimation in the urban environment rather than the rural environment, with a low IE value (approximately. 0.05 bits) ranging from the impervious fraction 60 to 95% and a high IE value (over 0.5 bits) from 5 to 50%. Figure 7(b)–7(f) demonstrates the variation of IE and condition IE over the entire impervious fraction range under the five study land zoning categories that verify the particular enhancement range of different land zoning categories. The gross dataset IE and IG curves are plotted in each figure to present the relationship between condition IE and IG, where the significant low condition IE is detected in a particular impervious fraction range of different land zoning categories, accompanied by the increase of IG.

Table 4 | Polynomial probability functions

Category	Polynomial probability functions	R^2
Gross dataset	$P(x) = -(7.783\times10^{-11})x^7 + (2.785\times10^{-8})x^6 - (3.986\times10^{-6})x^5 + (2.891\times10^{-4})x^4 - 0.01113x^3 + 0.2208x^2 - 2.008x + 7.479$	0.9992
High-density residential and commercial	$P(x) = (5.503\times10^{-11})x^7 - (1.816\times10^{-8})x^6 + (2.379\times10^{-6})x^5 - (1.566\times10^{-4})x^4 + 0.005445x^3 - 0.09524x^2 + 0.7171x - 1.366$	0.9995
Low- to medium-density residential	$P(x) = (1.147\times10^{-12})x^7 + (1.403\times10^{-9})x^6 - (4.862\times10^{-7})x^5 + (5.426\times10^{-5})x^4 - (2.581\times10^{-3})x^3 - 0.05464x^2 - 0.4518x + 1.006$	0.9998
Industrial	$P(x) = (3.621\times10^{-16})x^{11} - (1.957\times10^{-13})x^{10} + (4.594\times10^{-11})x^9 - (6.143\times10^{-9})x^8 + (5.157\times10^{-7})x^7 - (2.825\times10^{-5})x^6 + 0.001018x^5 - 0.0237x^4 + 0.3417x^3 - 2.812x^2 + 11.33x - 15.29$	0.9993
Urban green land	$P(x) = (5.33\times10^{-16})x^{11} - (3.209\times10^{-13})x^{10} + (8.468\times10^{-11})x^9 - (1.286\times10^{-8})x^8 + (1.242\times10^{-6})x^7 - (7.951\times10^{-5})x^6 + 0.003408x^5 - 0.09652x^4 + 1.736x^3 - 18.24x^2 + 93.22x - 124.8$	0.9993
Urban road	$P(x) = -(3.412\times10^{-16})x^{11} + (1.851\times10^{-13})x^{10} - (4.366\times10^{-11})x^9 + (5.872\times10^{-9})x^8 - (4.962\times10^{-7})x^7 + (2.739\times10^{-5})x^6 - 0.0009951x^5 + 0.02339x^4 + 0.3409x^3 + 2.836x^2 + 11.5x + 15.57$	0.9996

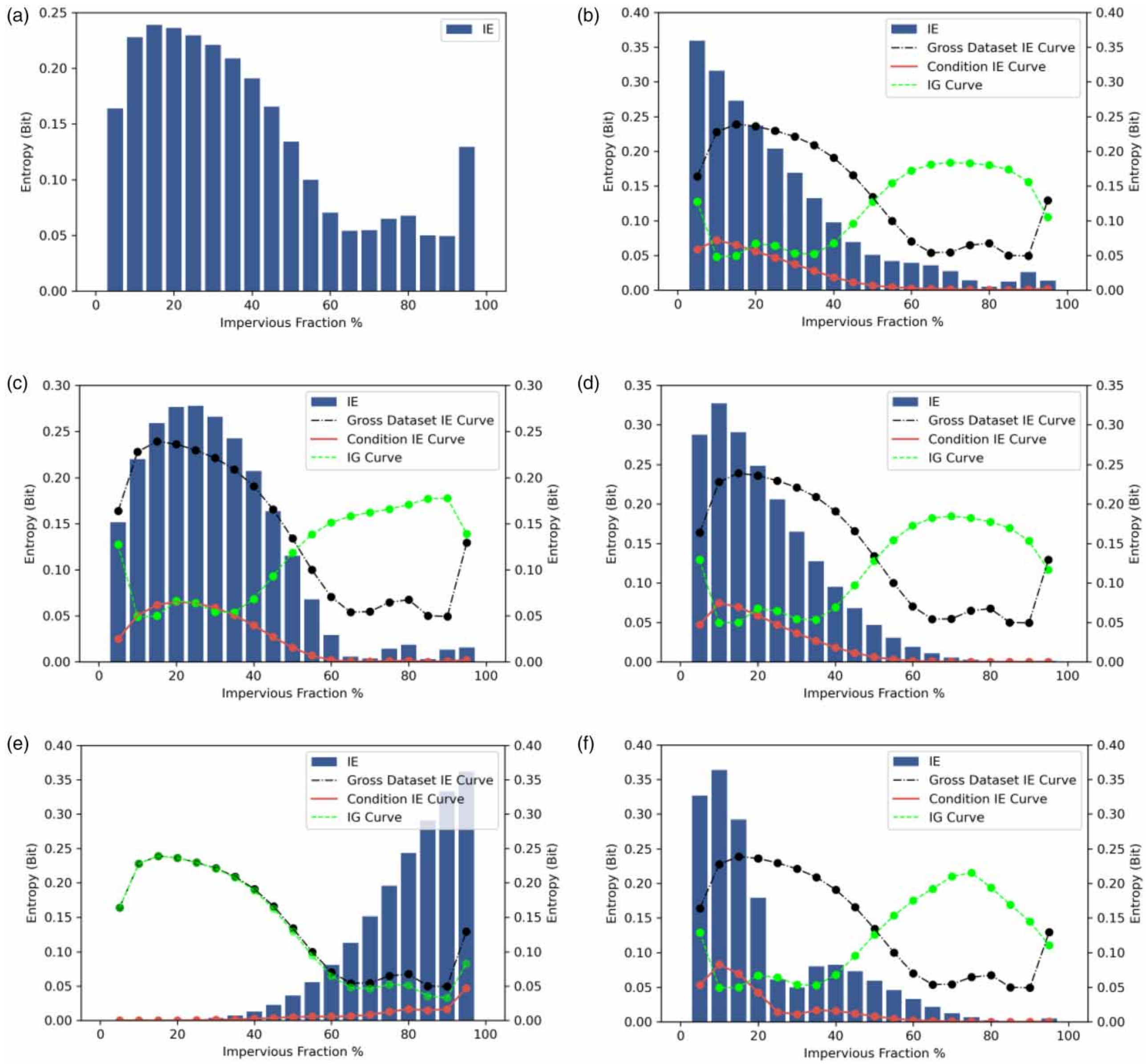

Figure 7 | IE, condition entropy and IG distributions: (a) Gross dataset, the prediction stability is in proportion to the impervious fraction. The lowest IE (0.048 bits) occurs at 85%; (b) High-density residential and commercial zone, the estimation is unstable between 0 and 50%, but robust between 70 and 90% with significant IG; (c) Low to medium-density residential zone, the prediction shows confident stability between 60 and 90% with a fluctuation at 80%, but not applicable from 0 to 50%; (d) Industrial zone, a significant climb of IG starts from 50% and reaches the top at 75%, with near-zero condition IE after 75%; (e) Urban green land zone, shows reversed distribution compared with the other categories. High stability occurs before 50% and low IG after 60%; and (f) Urban road zone, the prediction shows a broader stability range from 55 to 100%, with a peak IG of 0.24 bits at 75%, representing the highest probability of road imperviousness.

4. CONCLUSION

This study presented an integrated data-driven approach to estimate the impervious fractions for selected five urban catchments in Sydney under five predefined land zoning categories and a designed stability testing procedure with IE theory. Remote sensing imagery and land zoning maps were obtained and preprocessed for DL-based image classification and land zoning-based impervious feature extraction. The clustering algorithm MeanShift and DNNs DeepLabV3+ were utilised to reduce pixel textural/spectral complexity and classify the LULC of the remote sensing imagery with an overall impervious features prediction accuracy of 0.9634. Then, the predicted LULC maps and preprocessed land zoning maps were spatially fused and transported to the first proposed 'fishnet' sampling layer to extract impervious features based on the spatial relation between LULC and associated land zoning categories. After that, for the probability-fitting study, the extracted impervious samples were grouped by different land zoning categories and optimised by two computational items: the area reduction factor and the LAI. Three elements, likelihood distribution, accumulated likelihood distribution and corresponding polynomial fitting curves of impervious fractions, were computed using the gross sample set and land zoning sample set under the probability-fitting study, demonstrating various intervals of centralised distribution and occurrence likelihood. Finally, the IE theory was introduced to evaluate the prediction stability and verify the contribution of land zoning to estimate particular impervious fraction ranges by quantifying their IE, condition IE and IG, where land zoning shows robust information enhancement power in reducing the IE of particular impervious ranges.

In the probability-fitting study, the occurrence likelihood distributions of impervious fractions are different due to the specified LULC characteristics of different land zoning categories, which means urban planning has a decisive effect on the imperviousness of a land lot. Therefore, given the environmental or development plan of a pre-developed catchment, the impervious fraction of a specific area within the catchment can be estimated using the proposed workflow in this study and then translated to parameters of catchment modelling systems for simulating the rainfall–runoff process of the catchment. This approach can also improve the scientific estimation of the impact of urbanisation. These impacts guide urban managers to reduce or avoid the corresponding flood risk in the functional subdivision of urban areas. Due to the mechanism of DL, the DNNs-based LULC classification and segmentation may be more or less affected by seasonal or phenological variations within the remote sensing imagery (Yuan *et al.* 2008). For example, the LAI was involved in this study to reduce the obstruction of the tree canopy while extracting underlying impervious features. The statistical relationship between land zoning categories and impervious fraction was built on the Australian regional database. The global land zoning scheme has not yet been assessed due to the limitation of data availability. In addition, the approach's robustness can be gradually improved with the increase of study samples based on the construction method of the probability-fitting study. In this study, the proposed approach has been evaluated from the perspective of DL and statistics. Nevertheless, hydrological validation, such as hydrograph prediction and model calibration, has not been considered in this study, as the focus of this study was the development of reproducible parameter values for a catchment model. Further research should focus on resolving the seasonal or phenological influence on LULC classification, examining more urban catchments to increase the approach's robustness and hydrological validation of the parameter values derived using the approach outlined herein. Furthermore, the IG from the land zoning dataset to urban imperviousness estimation should be explored further using the database with different land zoning schemes. In summary, the efficacy and overall accuracy of the impervious fraction estimation approach are determined by both LULC prediction accuracy and sample amount, as well as the knowledge and experience of the modeller for applicable scenario selection. Although it is impossible to explore the comprehensive urban environment in one paper, this study clarifies the differences in estimating urban catchment impervious fraction under different land zoning categories.

ACKNOWLEDGEMENTS

The support of the City of Sydney Council, Sydney, Australia, is gratefully acknowledged. The remote sensing imagery and land zoning map are provided by NSW Spatial Service and Environmental Data Portal of Australia NSW Government.

DATA AVAILABILITY STATEMENT

Data cannot be made publicly available; readers should contact the corresponding author for details.

CONFLICT OF INTEREST

The authors declare there is no conflict.

REFERENCES

Andersen, N. 2013 *The Urban Community: A World Perspective*. Routledge, London.

Atkinson, P. M. & Curran, P. J. 1997 Choosing an appropriate spatial resolution for remote sensing investigations. *Photogrammetric Engineering and Remote Sensing* **63** (12), 1345–1351.

Ball, J., Babister, M., Nathan, R., Weinmann, P., Weeks, W., Retallick, M. & Testoni, I. 2019 *Australian Rainfall and Runoff-A Guide to Flood Estimation*. Commonwealth of Australia (Geoscience Australia), Canberra.

Beven, K. J. 2012 *Rainfall-runoff Modelling: the Primer*, 2nd edn. John Wiley and Sons, Chichester, UK.
Boyd, M., Bufill, M. & Knee, R. 1993 Pervious and impervious runoff in urban catchments. *Hydrological Sciences Journal* **38** (6), 463–478.
Byrne, J., Sipe, N. & Dodson, J. 2014 *Australian Environmental Planning: Challenges and Future Prospects*, Routledge, London.
Caves, R. W. 2004 *Encyclopedia of the City*. Routledge, London.
Chen, J. M. & Black, T. 1992 Defining leaf area index for non-flat leaves. *Plant, Cell & Environment* **15** (4), 421–429.
Chen, J., Hill, A. A. & Urbano, L. D. 2009 A GIS-based model for urban flood inundation. *Journal of Hydrology* **373** (1–2), 184–192.
Chen, L.-C., Papandreou, G., Schroff, F. & Adam, H. 2017 Rethinking atrous convolution for semantic image segmentation. *arXiv preprint arXiv:1706.05587*. Available from: https://arxiv.org/abs/1706.05587.
Chen, L.-C., Zhu, Y., Papandreou, G., Schroff, F. & Adam, H. 2018 *Encoder-decoder with Atrous Separable Convolution for Semantic Image Segmentation*. Paper presented at the Computer Vision - ECCV 2018, Cham Switzerland, pp. 833–851.
Chevrel, M., Courtois, M. & Weill, G. 1981 The SPOT satellite remote sensing mission. *Photogrammetric Engineering and Remote Sensing* **47**, 1163–1171.
Choi, K.-s. & Ball, J. E. 2002 Parameter estimation for urban runoff modelling. *Urban Water* **4** (1), 31–41.
City of Parramatta Council. 2011 *Parramatta Local Environmental Plan 2011*. City of Parramatta Council, Parramatta, NSW. Available from: https://www.cityofparramatta.nsw.gov.au/development/local-environmental-plans
City of Ryde Council. 2014 *Ryde Local Environmental Plan (LEP) 2014*. City of Ryde Council, Ryde, NSW. Available from: https://www.ryde.nsw.gov.au/Business-and-Development/Planning-Controls/Local-Environmental-Plan
City of Strathfield Council. 2012 *Strathfield City Local Environmental Plan (LEP) 2012*. Strathfield City Council, Strathfield, NSW. Available from: https://www.strathfield.nsw.gov.au/develop/shaping-strathfield-lep-2021/
City of Sydney Council. 2012 *Sydney Local Environmental Plan*. City of Sydney Council, Sydney, NSW. Available from: https://www.cityofsydney.nsw.gov.au/local-environmental-plans
City of Willoughby. 2012 *Willoughby Local Environmental Plan 2012*. Willoughby City Council, Chatswood, NSW. Available from: https://www.willoughby.nsw.gov.au/Development/Plan/Planning-Rules/WLEP
Comaniciu, D. & Meer, P. 2002 Mean shift: a robust approach toward feature space analysis. *IEEE Transactions on Pattern Analysis and Machine Intelligence* **24** (5), 603–619.
Dial, G., Bowen, H., Gerlach, F., Grodecki, J. & Oleszczuk, R. 2003 IKONOS satellite, imagery, and products. *Remote Sensing of Environment* **88** (1–2), 23–36.
Duranton, G. & Puga, D. 2015 Urban land use. In: *Handbook of Regional and Urban Economics*, Vol. 5. Elsevier, London, pp. 467–560.
Flanagan, M. & Civco, D. L. 2001 Subpixel impervious surface mapping. In: *Paper Presented at the Proceedings of the 2001 ASPRS Annual Convention. St. Louis, MO, USA*.
Geoscience Australia 2022 *OzWALD Gridded Environmental Data for Australia (Annual Mean Leaf Area Index)*. Available from: https://portal.ga.gov.au/
Gong, S., Ball, J. & Surawski, N. 2022 Urban land-use land-cover extraction for catchment modelling using deep learning techniques. *Journal of Hydroinformatics* **24** (2), 388–405.
Grimond, J. 2007 *The World Goes to Town: A Special Report on Cities*. *Economist Newspaper*. https://www.economist.com/special-report/2007/05/03/the-world-goes-to-town.
Gurran, N., Gilbert, C. & Phibbs, P. 2015 Sustainable development control? zoning and land use regulations for urban form, biodiversity conservation and green design in Australia. *Journal of Environmental Planning and Management* **58** (11), 1877–1902.
He, N., Fang, L. & Plaza, A. 2020 Hybrid first and second order attention Unet for building segmentation in remote sensing images. *Science China Information Sciences* **63** (4), 1–12.
Huang, S., Wang, H., Xu, Y., She, J. & Huang, J. 2021 Key disaster-causing factors chains on urban flood risk based on Bayesian network. *Land* **10** (2), 210.
Jamali, B., Löwe, R., Bach, P. M., Urich, C., Arnbjerg-Nielsen, K. & Deletic, A. 2018 A rapid urban flood inundation and damage assessment model. *Journal of Hydrology* **564**, 1085–1098.
Jensen, J. R. & Cowen, D. C. 1999 Remote sensing of urban/suburban infrastructure and socio-economic attributes. *Photogrammetric Engineering and Remote Sensing* **65**, 611–622.
Jiang, J. 2010 *Large Sample Techniques for Statistics*. Springer, New York.
Johnston, R. M. & Barson, M. M. 1993 Remote sensing of Australian wetlands: an evaluation of Landsat TM data for inventory and classification. *Marine and Freshwater Research* **44** (2), 235–252.
Kiran, T. T. J. 2020 Computer vision accuracy analysis with deep learning model using tensorFlow. *International Journal of Innovative Research in Computer Science & Technology (IJIRCST)* **8** (4), 115–123. http://dx.doi.org/10.2139/ssrn.3673214.
Kuczera, G. & Parent, E. 1998 Monte Carlo assessment of parameter uncertainty in conceptual catchment models: the Metropolis algorithm. *Journal of Hydrology* **211** (1–4), 69–85.
Li, W., Liu, H., Wang, Y., Li, Z., Jia, Y. & Gui, G. 2019 Deep learning-based classification methods for remote sensing images in urban built-up areas. *Ieee Access* **7**, 36274–36284.
Malz, A. M. 1997 Estimating the probability distribution of the future. *Journal of Derivatives* **5** (2), 18–36.
Mason, P. 2012 Zoning, land-use planning and tourism. In: *The Routledge Handbook of Tourism and the Environment*. Routledge, London, pp. 288–297.

Metropolis, N. & Ulam, S. 1949 The monte carlo method. *Journal of the American Statistical Association* **44** (247), 335–341.

Mohapatra, R. P. & Wu, C. 2010 High resolution impervious surface estimation. *Photogrammetric Engineering & Remote Sensing* **76** (12), 1329–1341.

National Research Council 2009 *Urban Stormwater Management in the United States*. National Academies Press, Washington, DC.

NSW Government 2021 *Local Environmental Plan Making Guideline*. NSW Government, Sydney. Available from: https://www.planning.nsw.gov.au/Plans-for-your-area/Local-Planning-and-Zoning

NSW Government Spatial Service 2021 *Historical, Aerial and Satellite Imagery*. Available from: https://www.spatial.nsw.gov.au/products_and_services/aerial_and_historical_imagery

Núñez, J., Cincotta, P. & Wachlin, F. 1996 Information entropy. In: Muzzio, J. C., Ferraz-Mello, S. & Henrard, J. (eds). *Chaos in Gravitational N-Body Systems*. Springer, Dordrecht, pp. 43–53.

Organisation for Economic Co-operation and Development Staff 2017 *Land-Use Planning Systems in the OECD: Country Fact Sheets*. OECD Regional Development Studies, OECD Publishing, Paris, https://doi.org/10.1787/9789264268579-en.

Rwanga, S. S. & Ndambuki, J. M. 2017 Accuracy assessment of land use/land cover classification using remote sensing and GIS. *International Journal of Geosciences* **8** (04), 611.

Salvadore, E., Bronders, J. & Batelaan, O. 2015 Hydrological modelling of urbanized catchments: a review and future directions. *Journal of Hydrology* **529**, 62–81.

Sim, J. & Wright, C. C. 2005 The kappa statistic in reliability studies: use, interpretation, and sample size requirements. *Physical Therapy* **85** (3), 257–268.

Slonecker, E. T., Jennings, D. B. & Garofalo, D. 2001 Remote sensing of impervious surfaces: a review. *Remote Sensing Reviews* **20** (3), 227–255.

Stehman, S. 1996 Estimating the kappa coefficient and Its variance under stratified random sampling. *Photogrammetric Engineering and Remote Sensing* **62** (4), 401–407.

Tokuda, K., Masuko, T., Miyazaki, N. & Kobayashi, T. 2002 Multi-space probability distribution HMM. *IEICE TRANSACTIONS on Information and Systems* **85** (3), 455–464.

Toutin, T. & Cheng, P. 2002 Quickbird–a milestone for high resolution mapping. *Earth Observation Magazine* **11** (4), 14–18.

Tripp Corbin, G. 2015 *Learning ArcGIS Pro*. Packt Publishing Ltd, Birmingham.

Van de Voorde, T., De Roeck, T. & Canters, F. 2009 A comparison of two spectral mixture modelling approaches for impervious surface mapping in urban areas. *International Journal of Remote Sensing* **30** (18), 4785–4806.

Volkenstein, M. V. 2009 Entropy and probability. In: *Entropy and Information. Progress in Mathematical Physics*, vol 57. Birkhäuser, Basel. https://doi.org/10.1007/978-3-0346-0078-1_4.

Vries, P. G. d. 1986 Stratified random sampling. In: *Sampling Theory for Forest Inventory*. Springer, Berlin, Heidelberg, pp. 31–55. https://doi.org/10.1007/978-3-642-71581-5_2.

Weih, R. C. & Riggan, N. D. 2010 Object-based classification vs. pixel-based classification: comparative importance of multi-resolution imagery. *The International Archives of the Photogrammetry, Remote Sensing and Spatial Information Sciences* **38** (4), C7.

Weng, Q. 2012 Remote sensing of impervious surfaces in the urban areas: requirements, methods, and trends. *Remote Sensing of Environment* **117**, 34–49.

Williams, D. L., Goward, S. & Arvidson, T. 2006 Landsat. *Photogrammetric Engineering & Remote Sensing* **72** (10), 1171–1178.

Wu, C. & Murray, A. T. 2003 Estimating impervious surface distribution by spectral mixture analysis. *Remote Sensing of Environment* **84** (4), 493–505.

Xu, Y., Wu, L., Xie, Z. & Chen, Z. 2018 Building extraction in very high resolution remote sensing imagery using deep learning and guided filters. *Remote Sensing* **10** (1), 144.

Yang, L., Xian, G., Klaver, J. M. & Deal, B. 2003 Urban land-cover change detection through sub-pixel imperviousness mapping using remotely sensed data. *Photogrammetric Engineering & Remote Sensing* **69** (9), 1003–1010.

Yuan, F., Wu, C. & Bauer, M. E. 2008 Comparison of spectral analysis techniques for impervious surface estimation using landsat imagery. *Photogrammetric Engineering & Remote Sensing* **74** (8), 1045–1055.

Yurtkulu, S. C., Sahin, Y. H. & Ünal, G. B. 2019 Semantic Segmentation with Extended DeepLabv3 Architecture. *2019 27th Signal Processing and Communications Applications Conference* (SIU), 1–4.

Zhang, C., Pan, X., Li, H., Gardiner, A., Sargent, I., Hare, J. & Atkinson, P. M. 2018 A hybrid MLP-CNN classifier for very fine resolution remotely sensed image classification. *ISPRS Journal of Photogrammetry and Remote Sensing* **140**, 133–144.

Zhou, Z., Rahman Siddiquee, M. M., Tajbakhsh, N. & Liang, J. 2018 Unet++: A nested u-net architecture for medical image segmentation. In: Maier-Hein, L., Syeda-Mahmood, T., Taylor, Z., Lu, Z., Stoyanov, D., Madabhushi, A., Tavares, J. M. R. S. Nascimento, J. C., Moradi, M., Martel, A., Papa, J. P., Conjeti, S., Belagiannis, V., Greenspan, H., Carneiro, G. & Bradley, A. (eds). *Deep Learning in Medical Image Analysis and Multimodal Learning for Clinical Decision Support - 4th International Workshop, DLMIA 2018 and 8th International Workshop, ML-CDS 2018 Held in Conjunction with MICCAI 2018* (pp. 3 –11). (Lecture Notes in Computer Science (including subseries Lecture Notes in Artificial Intelligence and Lecture Notes in Bioinformatics); Vol. 11045 LNCS). Springer Verlag. https://doi.org/10.1007/978-3-030-00889-5_1.

First received 30 September 2022; accepted in revised form 17 February 2023. Available online 2 March 2023